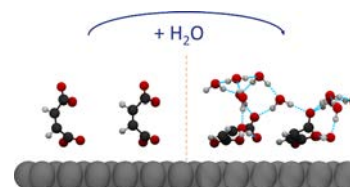


Role of the Hydration Shell in the pH-Dependent Adsorption of Maleic Acid

Nils Schewe, Robin Wagner, Matthias Franzreb, and Peter Thissen*

ABSTRACT: Past model studies have investigated adsorption processes on carbonaceous surfaces, focusing on gas phase adsorption and thus uncharged molecules. In real world applications, the adsorption from solutions is oftentimes of higher interest though, bringing charged species into the equation. In aqueous solutions, the first water layer with its stabilizing hydrogen bonds is especially important for the overall stability of the system. In this study, we use ab initio density functional theory for modeling the adsorption of (charged) maleic acid on a graphene sheet along with experimental validation of the computational results. We find that including a water layer makes a substantial difference in the conformation of charged adsorbed molecules. The results obtained are also in good agreement with the corresponding experiments.



1. INTRODUCTION

To separate and concentrate charged organic molecules from dilute solutions, the application of adsorption processes is recently getting increased attention.^{1–5} In these processes, the solution is brought into contact with a highly porous three dimensional sponge of an adsorptive material. In the past 10 years, graphene has gained attention due to its applicability in several different fields. Furthermore, activated carbonaceous surfaces have been used in adsorptive processes for a long time due to their high specific surfaces and low cost.⁶

The adsorption of small organic molecules on fractions of graphene surfaces from the gas phase has been studied for a number of molecules like acetone, acetonitrile, dichloro methane, and more.^{7–10} It has been shown that dispersion interactions play a major role in these processes. Nonlocal effects on graphene have been investigated as well,¹¹ showing their importance. Notably, these studies focused on adsorption from the gas phase and often used semiempirical auxiliaries to reduce simulation times. We introduce a layer of water to the system to enhance the comparability between an experiment and a calculation. As will become evident in this study, using gas phase adsorption yields curious results when the adsorbate is charged. Thus, the introduction of a hydration shell is obligatory.¹² Solvent layers of this kind are also important to, e.g., understand the interactions between enzymes and their environment. This is of high importance for the application of enzymes in catalytic systems or biomedical and biotechnological applications. Being able to fine tune interactions between proteins and (negatively) charged polymers through the integrative use of computational design, protein re engineering and biophysical characterization proved to be essential to improve chemical reaction performance.^{13–16}

To exemplarily demonstrate the advantages of ab initio computational modeling in industrially relevant processes, the

extraction of maleic acid (MA) from reaction media by sorption was approached both theoretically and experimentally. The respective contemplations made in this work combine engineering and surface and theoretical chemistry. In this work, we present an experimentally validated ab initio approach for the determination of the thermodynamic adsorption properties of maleic acid and its anions on carbonaceous surfaces. The adsorption has been modeled for a graphene surface layer with different degrees of surface coverage by maleic acid in different dissociation states and a dynamic water layer. The presented approach is generalizable and can thus be used to predetermine the adsorption behavior of (polar) organic molecules on nonmetallic surfaces.

2. METHODS

2.1. Computational Methods. All ab initio density functional theory (DFT) calculations were performed using the Vienna Ab initio Simulation Package (VASP).¹⁷ For the majority of the calculations, the GPU port of VASP was used.^{18,19} It is to be noted that in our case, GPU acceleration led to about 4 fold faster calculations. For the electronic interactions, the projector augmented wave (PAW) method was employed.²⁰ Restricting parameters were set to a kinetic energy cutoff of 360 eV and $4 \times 4 \times 1$ Monkhorst–Pack²¹ k points. Structures were relaxed to residual stress below 0.01 eV/Å. The approximation of electron–electron exchange and

correlation energies were included via the generalized gradient approximation (GGA).²² For charged systems, a ubiquitous background charge has been assumed (i.e., electrons were added to the cell to match the desired charge state). To correct the dispersion, the DFT D3 method by Grimme with damping according to Becke and Jonson was chosen.^{23,24} In systems with graphene sheets, van der Waals interactions are crucial. The necessary number of k points for a realistic representation of graphene was determined via the comparison of the number of k points, the duration of the calculation, and the resulting bond lengths and angles. It was found that a setting of $4 \times 4 \times 1$ k points along the graphene plane already yielded realistic graphene while keeping computation times reasonable. The supercells were constructed to have headspace (vacuum) between the graphene layers to morph three dimensional periodicity into graphene slabs with effective two dimensional periodicity. The cell used in the calculations had dimensions of $14.76 \text{ \AA} \times 8.52 \text{ \AA} \times 14.00 \text{ \AA}$ with a maximum of 108 atoms. For the 48 graphene carbon atoms per cell, a mean C–C bond length of $1.4202 \pm 0.0004 \text{ \AA}$ and a mean bond angle of $120.00 \pm 0.01^\circ$ were found, equal to literature values.²⁵

2.2. Adsorption Experiments. The adsorption experiments were conducted in batch mode by incubating the carbon powder with a maleic acid solution of varying concentrations and pH values. As the carbon powder, we chose the activated carbon Carbopal SC11PG from Donau Carbon (Frankfurt, Germany). We characterized it via Brunauer–Emmett–Teller (BET) measurement with a Gemini VII 2390 from Micrometrics Instrument Corp. (Norcross), which yielded a specific surface area of $909 \text{ m}^2/\text{g}$, an average pore size of 1.83 nm , and an average particle size of $37.6 \text{ }\mu\text{m}$. To initiate the experiment, 20 mg of the activated carbon powder was mixed with 1.5 mL of a maleic acid solution, which was prepared from maleic acid ($\geq 99\%$, Merck, Darmstadt, Germany). The initial ratio of maleic acid to the carbon material was varied ($0.75, 1.125, 1.5, 1.875, \text{ and } 2.25 \text{ mmol/g}$, matching $10, 15, 20, 25, \text{ and } 30 \text{ mmol/L}$, respectively). For pH dependent loading experiments, the pH (range $2\text{--}10$) was adjusted using NaOH (2 M aq., Merck, Darmstadt, Germany). For equilibration, the carbon powder was mixed with the solution in a 2 mL Eppendorf cup and incubated in a thermomixer (Thermomixer comfort, Eppendorf Hamburg, Germany), shaking at 1000 rpm for 24 h at room temperature. After centrifugation of the reaction vessels at 8000 rpm for 1 min , the supernatant was extracted and filtered through a $0.45 \text{ }\mu\text{m}$ poly (tetrafluoroethylene) (PTFE) syringe filter. Afterward, the maleic acid concentration of the solution was determined photometrically with an EnSpire Multimode Plate Reader (PerkinElmer, Waltham) at a wavelength of 254 nm . The experiments were conducted at least twice for every condition to ensure reproducibility.²⁶

2.3. Isotherm Model and Parameter Determination. Due to the influence of the pH on the loading of carbon with maleic acid and the pH shift occurring during the adsorption process, it is almost impossible to determine an isotherm for a specific pH without using buffers. Furthermore, due to (partial) dissociation, there are two maleic acid species present at most pH values simultaneously, leading to the adsorption of two different species for most pH values. To simplify the description, we refer to the different species as A for the uncharged species ($\text{C}_4\text{O}_4\text{H}_4$), B for the 1 fold negatively charged species ($\text{C}_4\text{O}_4\text{H}_3^-$), and C for the 2 fold negatively charged species ($\text{C}_4\text{O}_4\text{H}_2^{2-}$). In the following, we will discuss

the case of a mixture of species A, B, and C in solution with concentrations c_A , c_B , and c_C respectively. To describe the loading of the carbon in equilibrium, we decided to use the multicomponent Langmuir model for single site adsorption processes, as described by Swenson and Stadie.²⁷ In this case, only one molecule can bind per adsorption site, and the adsorption affinity between the carbon material and the ions is considered in the affinity constants K_A , K_B , and K_C (comp. Table 1).

Table 1. Affinity Parameters of the Multicomponent Langmuir Model for the Adsorption of Maleic Acid on Carbopal SC11PG Activated Carbon

	MA on carbopal SC11PG
parameter	GA
K_A (L/mol)	8398.1
K_B (L/mol)	130.6
K_C (L/mol)	14.5
q_{max} (mmol/g)	1.20
R^2	0.93

When species A, B, and C are present, the loading ratio of A to the maximum loading (or the total amount of binding sites) is given by

$$\frac{N_A}{N_{\text{max}}} = \frac{q_A}{q_{\text{max}}} = \frac{c_A K_A}{1 + c_A K_A + c_B K_B + c_C K_C} \quad (1)$$

The total amount of maleic acid adsorbed to the carbon material can be simply calculated by the addition of the loadings of the present species. The loading of the carbon material can then be determined for the whole pH range

$$\frac{N_A + N_B + N_C}{N_{\text{max}}} = \frac{q_{\text{ges}}}{q_{\text{max}}} = \frac{c_A K_A + c_B K_B + c_C K_C}{1 + c_A K_A + c_B K_B + c_C K_C} \quad (2)$$

It is necessary to find four parameters to solve this equation. To determine the most reasonable affinity constants and the corresponding q_{max} , a fitting algorithm between the parameters and all our experimental data is needed, representing a variety of equilibrium conditions and, consequently, all data for all different maleic acid species. Thus, it is impossible to determine the parameters successively. A method we found to be suitable is the genetic algorithm (GA), which is known to be able to fit several independent parameters to the experimental data simultaneously.²⁸

For setting up the genetic algorithm, we started with 10 parameter sets consisting of random numbers for each of the requested parameters. The range for the random generation of the adsorption constants was set from 0 to 10^5 L/mol and for q_{max} between 0 and 1.5 mmol/g . These parameter sets and the equilibrium conditions of all experiments N_{exp} were used to calculate the loading q_{calc} (eq 2). The results were then compared with the experimentally determined loadings q_{exp} of the carbon material by determining the fitness of each parameter set using the objective function, which in this case was the coefficient of determination^{29,30}

$$R^2 = 1 - \frac{\sum_{i=1}^{N_{\text{exp}}} (q_{\text{calc},i} - q_{\text{exp},i})^2}{\sum_{i=1}^{N_{\text{exp}}} (q_{\text{exp},i} - \bar{q}_{\text{exp}})^2} \quad (3)$$

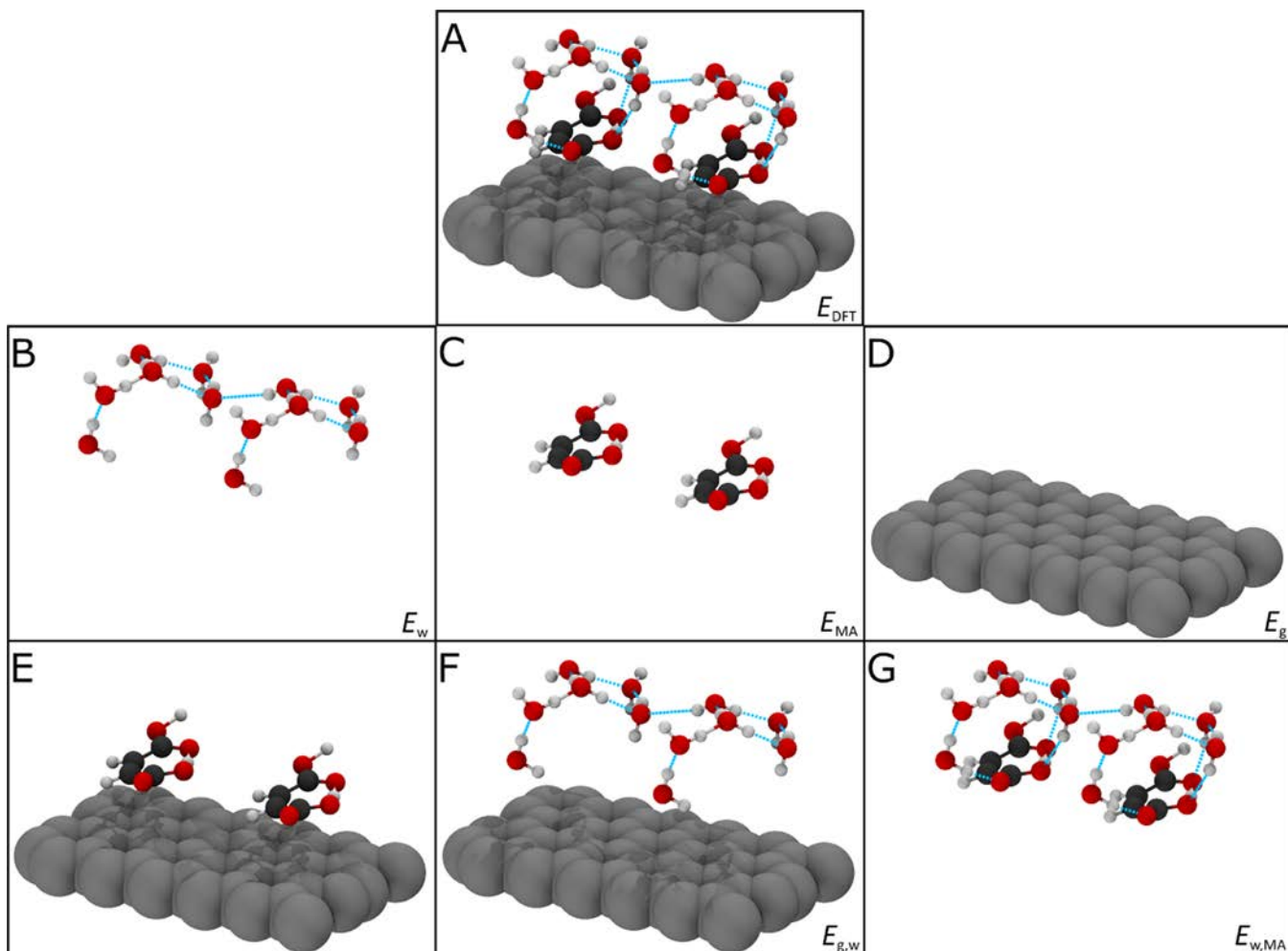


Figure 1. Cell [2–00] containing two undissociated molecules of maleic acid, a graphene sheet, and 12 molecules of water (A) and all subsequent partial structures (B–G) with the respective energies as used in eqs 4–6. (B) Isolated maleic acid structure; (C) isolated maleic acid structure; (D) isolated graphene sheet; (E) graphene sheet with maleic acid structure; (F) graphene sheet with water structure; and (G) maleic acid and water. Graphene carbon atoms are displayed in anthracite, maleic acid carbon atoms are displayed in black, oxygen atoms are displayed in red, hydrogen atoms are displayed in light gray, and hydrogen bonding is displayed in cyan.

According to the definition, the parameter set with the highest accordance to the experimental data yields the R^2 closest to 1. Under this premise, the parameter sets were ranked. Nine new parameter sets were created by pairing the five best parameter sets. In addition, some parameters were replaced by a randomly generated value in the defined range with a mutation probability of 20%. Only the best parameter set was kept without any changes for the next evaluation step. To find the best fit with high probability, the procedure was repeated 200 000 times. The resulting parameters are presented in Table 1.

3. RESULTS

3.1. Computational Results. To gain an initial understanding of the interaction between the carbonaceous surface and the maleic acid, a DFT study of a model system was conducted. In this, we specifically investigate the adsorption properties of the maleic acid and the pH dependent grand canonical potential of the model cells. For an effective representation of the adsorbent surface, we use a graphene sheet covered with different amounts of maleic acid and a water layer to mimic the first hydration shell. Graphene as a surface slab has some distinct electronic properties that require

special caution when conducting calculations. Along the plane, graphene is a zero band gap semiconductor with a double cone shaped band structure. This makes it factually conductive along the sheet. Along the plane normal though, graphene behaves like an insulator or a semiconductor with a large band gap—the exact value depends on the number of layers that are stacked.^{25,31,32}

For the DFT calculations, an orthorhombic cell was chosen. The dimensions of the xy plane were prepared to match the periodicity of the graphene layer. Graphene was loaded with 12 molecules of water and 1 or 2 molecules of maleic acid to simulate different surface coverages (50 and 99%). Maleic acid was gradually deprotonated and the cell was charged accordingly to image different pH values of the surrounding medium. Afterward, all energies of the subparts (water/graphene/maleic acid) and their combinations were recalculated by removing all other atoms from the cells and fixing the atom positions (comp. Figure 1). To describe the cell configurations, we use a nomenclature of the form $[x-yz]$, with x being the number of molecules of maleic acid per cell (either 1 or 2) and y and z describing the degree of dissociation of the respective molecules of maleic acid. For example, the cell containing one molecule of maleic acid with

Table 2. Distribution of the Negative Charge inside the Given Cell Configuration on the Respective Substructure in Percent^a

cell	1 01	1 02	2 01	2 02	2 11	2 12	2 22
neg. charge/e	1.000001	2.000005	1.000003	1.999995	2.000005	3.000006	4.000003
graphene/%	95.58	53.56	93.71	53.70	60.33	46.82	53.70
water/%	3.35	16.76	2.87	15.12	14.79	22.03	15.12
maleic acid/%	1.07	29.68	3.41	31.18	24.89	31.15	31.18

^aThe column header describes the cell configuration with the number of maleic acid molecules per cell at first, followed by the dissociation state of the molecules.

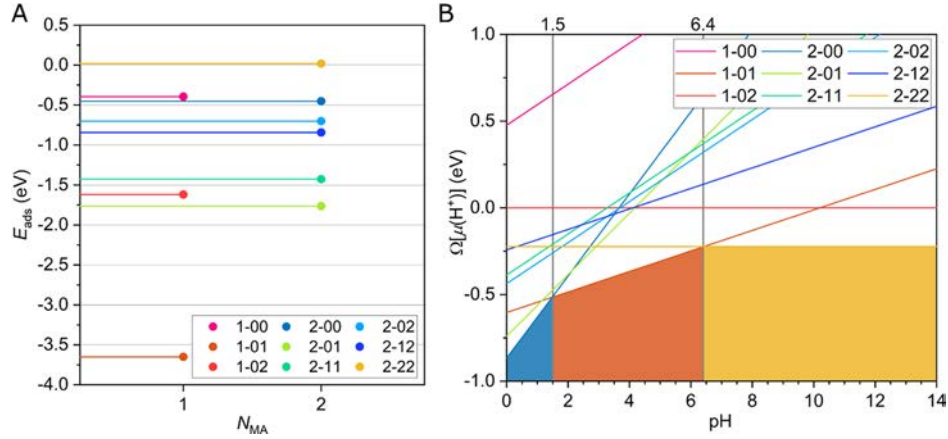


Figure 2. (A) Adsorption energies of maleic acid on graphene for all studied DFT cell configurations. (B) pH dependent grand canonical potentials of all cell configurations in dependency of the pH. Lower values are more favorable.

one proton dissociated (and thus carrying 1 electron equivalent of negative charge) is described as [1–01].

In an isolated system, the total energy is equal to the sum of the energy of its parts and the interaction energy between these parts. To extract the adsorption energy E_{ads} of maleic acid on graphene from a system that also contains water, not only the energy of the water structure E_w , graphene sheet E_g , and maleic acid E_{MA} but also their respective interactions have to be subtracted out of the total cell energy.

For this, we use a comparison of the cell energies following eqs 4–6

$$E_{\text{ads}} = \frac{E_{\text{DFT}} - E_g - E_w - E_{\text{MA}} - E_{\text{hydr}} - E_{\text{ghydr}}}{N_{\text{MA}}} \quad (4)$$

with

$$E_{\text{hydr}} = E_{w,\text{MA}} - E_w - E_{\text{MA}} \quad (5)$$

and

$$E_{\text{ghydr}} = E_{g,w} - E_g - E_w \quad (6)$$

In detail, the adsorption energy E_{ads} (eq 4) between maleic acid and the graphene surface is obtained by subtracting the energy of the graphene sheet E_g (Figure 1D), the energy of the water structure E_w (Figure 1B), the energy of the corresponding molecules of maleic acid E_{MA} (Figure 1C), the hydration energy E_{hydr} between water and maleic acid, and the interaction energy E_{ghydr} between water and graphene from the total cell energy E_{DFT} (Figure 1A). Division by the number of molecules of maleic acid N_{MA} leaves the adsorption energy per molecule. Hydration energy E_{hydr} (eq 5) is calculated from the subcell containing water and maleic acid $E_{w,\text{MA}}$ (Figure 1G), the one with only water E_w (Figure 1B), and the one with only maleic acid E_{MA} (Figure 1C). The interaction energy between water and graphene E_{ghydr} (eq 6) is calculated from

the subcell containing water and graphene $E_{g,w}$ (Figure 1F), the one with only graphene E_w (Figure 1D), and the one with only water E_w (Figure 1A). The cell with the graphene sheet and only maleic acid (Figure 1E) is not used in the calculation but shown for completion.

For every cell configuration, the subparts of that specific cell are used for the calculation. This ensures accurate and comparable results between cells of different charge density distributions, stoichiometries, and overall structures. To assign the correct charge densities when recalculating the energies of the subparts of each cell, Bader charge analysis (BCA)³³ of all structures has been conducted after initial relaxation of the full structure (e.g., Figure 1A). This was carried out both with and without background charge equivalent to the degree of dissociation for each cell and with fixed atom positions (self consistent step). This showed a charge density distribution different from what was expected (comp. Table 2), that is, instead of the majority of the charge being located on the carboxyl groups of maleic acid, a considerable amount, namely, 46.82–95.58% of the total cell charge, was delocalized on the graphene layer. The hydration shell buffered between 2.87 and 22.03% of the total cell charge. This led to maleic acid only carrying 1.07–31.18% of the total cell charge. Importantly, the percental charge delocalized on graphene was the highest for low total (negative) charges of the cell—graphene stabilized around 1 electron equivalent of charge in most configurations.

For the uncharged cells ([1–00] and [2–00]), a charge distribution close to the theoretical values given by the number of valence electrons is found. In the [1–00] cell, the graphene sheet carries a positive charge of $-0.06 e^-$, the MA carries a negative charge of $0.09 e^-$, and the water structure carries the remaining positive charge of $-0.06 e^-$. In the [2–00] cell, the graphene sheet carries a positive charge of $-0.09 e^-$, the MA carries a negative charge of $0.19 e^-$, and the water structure carries the remaining positive charge of $-0.10 e^-$.

After the aforementioned steps, the obtained adsorption energies (Figure 2A) are in the range of -3.65 – 0.02 eV, with negative values describing attractive interaction. The cells with two molecules of maleic acid yielded overall weaker (less negative) adsorption energies than the ones with only one molecule of maleic acid. The adsorption energy, however, is only a part of the picture, as will be discussed later (comp. Figure 2B, grand canonical potential).

3.2. Distance/Orientation between Maleic Acid and Graphene. The distance and orientation of maleic acid relative to the graphene sheet provide insights into the nature of their main interaction. Comparing all relaxed structures, what stands out most is that in the undissociated (and therefore uncharged) cases, the aliphatic backbone of maleic acid is closer to graphene than carboxylic acid groups. Upon dissociation (and charging), this flips around, leaving the carboxylic groups the closest to the graphene sheet. This is neatly displayed in the minimal distances (Table 3), where the shape of the molecule in the adsorbed state is also listed as the configuration.

Table 3. Distance between Maleic Acid and the Graphene Sheet Per Cell Configuration and Molecule^a

cell	config. 1	closest atom 1	distance 1 (Å)	config. 2	closest atom 2	distance 2 (Å)
1 00				p	C bb	3.12
1 01				p	O ac	3.13
1 02				a	O ac	2.97
2 00	p	C bb	3.12	p	C bb	3.12
2 01	p	C bb	3.13	p	O ac	3.17
2 02	p	O ac	3.08	a	O ac	2.95
2 11	p	O ac	3.05	p	O ac	2.98
2 12	c	O ac	3.07	a	O ac	2.74
2 22	a	O ac	2.88	a	O ac	2.82

^aConfig. = shape of the molecule; bb = backbone; ac = acid; p = planar (Figure 3A); c = curved (Figure 3B); and a = angled (Figure 3C).

When only dissociating one acidic proton, maleic acid tends to keep its initial planar shape, in some cases curving away from the surface by a few degrees (Figure 3A,B). This is mainly due to the O–H–O group in the middle of the molecule, which bridges the two carboxylic acid groups. Upon dissociation of the second proton, this bridge is opened, and

the acid groups rotate away from the molecular plane. This rotation causes one (or two) of the oxygen atoms to come closer to the graphene sheet (Figure 3C). It also results in more effective interaction with the hydration shell. In Figure 3, the water structure has been occluded to aid the visibility of the molecular shapes. Importantly, the structures shown stem from relaxation with the water layer.

3.3. Hydration Shell. The deconvolution of the cell's substructure's energies gives the opportunity to look into additional details. For example, a closer look at the water structure shows that in the majority of the examined configurations, a dense net of hydrogen bonds is formed, which even exceeds the cell limits (along the xy plane). From the isolated water substructures (comp Figure 1B), via division of the energy of this structure E_w by the number of water molecules in the cell $N_w = 12$, the average chemical potential per water molecule can be estimated. This, after referencing against solid water (ice_{th}), results in $\mu_{\text{H}_2\text{O},r} = 0.325$ eV and thus falls right between the theoretical value for the gas phase ($\mu_{\text{H}_2\text{O},\text{gas},r} = 0.614$ eV) and the reference value for the solid phase water ($\mu_{\text{H}_2\text{O},\text{solid},r} = 0$ eV), as reproduced according to the literature.³⁴ Therefore, our system can be expected to be a good model for a surface covered by a layer of liquid water.

The energy of the hydration shell in turn has a great influence on the molecule's adsorption behavior. In general, adsorption only really becomes favorable when it grants energy compared to the full hydration shell in solution. Although additional effects like entropy are not considered in this study, comparing the interaction energy between the water structure and maleic acid to the adsorption energy provides an anchor point for comparison to the experimental findings. Since water is a polar substance that readily forms hydrogen bonds with adjacent molecules, the charge dependency of the interaction energy between maleic acid and the water structure is expected. Namely (Figure 4A), above a minimal charge per molecule of maleic acid (gray area), the hydration energy E_{hydr} becomes more negative with a higher charge per molecule. This is in accordance with a study by Hafshejani.³⁵ There are two main reasons for this trend: first, the higher charge is accompanied by deprotonation of the acid groups, leading to higher susceptibility to hydrogen bonding, and second, as was shown above, the geometry of the organic molecule changes. The rotation of the carboxylic groups against the molecular plane and toward water leads to higher accessibility thereof and

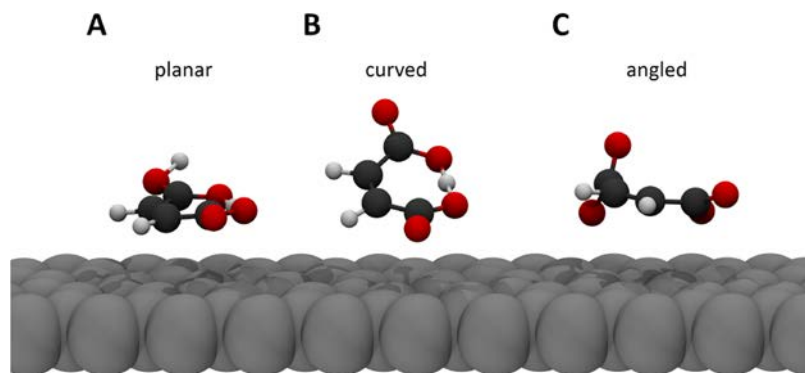


Figure 3. Shapes of maleic acid in the adsorbed state depending on the degree of dissociation (comp. Table 3). (A) The undissociated molecule in the planar configuration; (B) one acidic proton dissociated, curved configuration; and (C) angled shape after dissociation of both acidic protons. Colors as in Figure 1, water structure occluded for clarity.

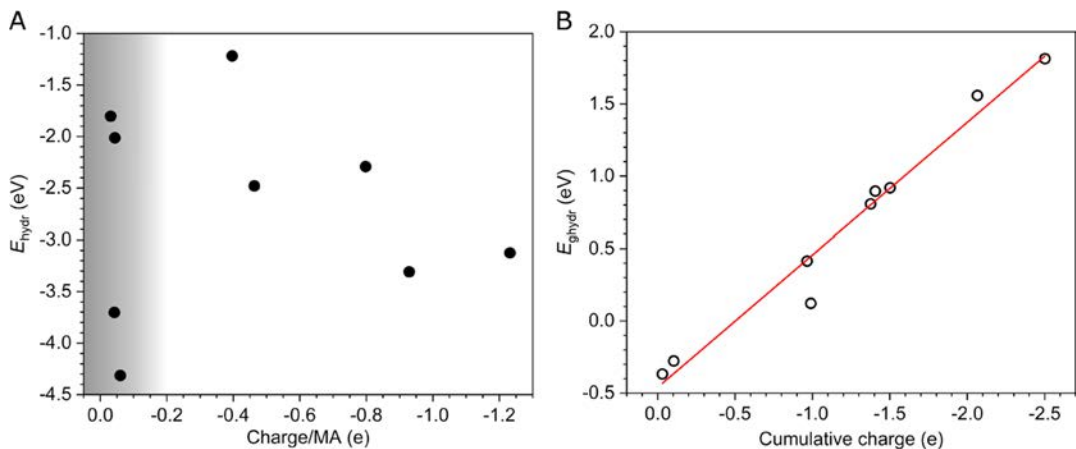


Figure 4. (A) Energy of hydration E_{hydr} in dependency of the water/maleic acid substructure's charge per molecule of maleic acid (MA) and (B) interaction energy between the water layer and graphene E_{ghydr} depending on the cumulative charge of water and graphene (comp. Table 2) with an indicative linear fit.

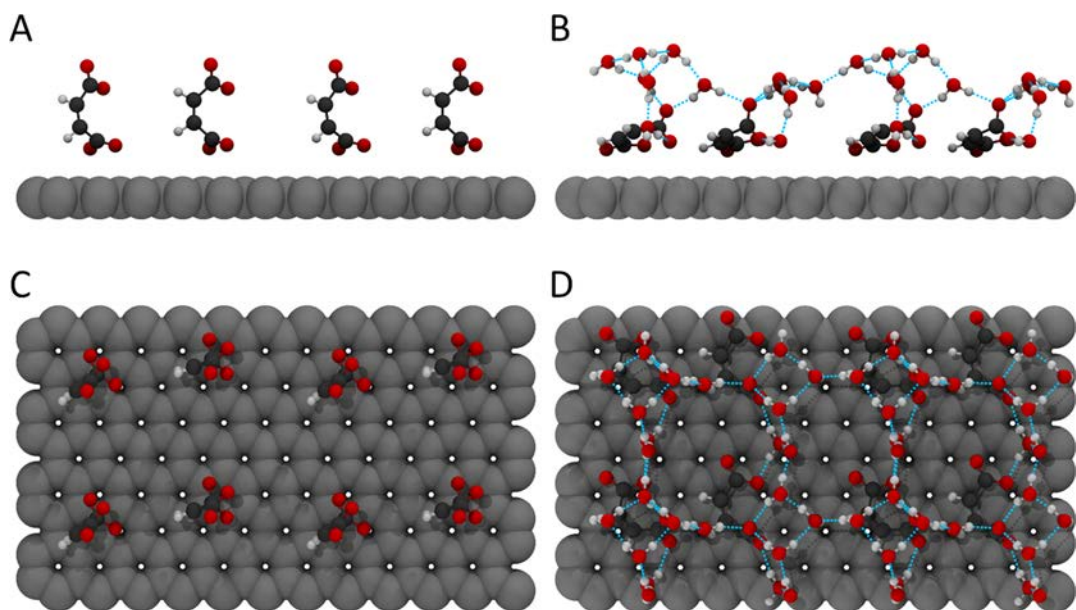


Figure 5. Modification of the [2-22] cell after relaxation with (B, D) and without (A, C) the hydration shell. The upper row shows the side view and the lower row shows the top view. Colors as in Figure 1.

thus to more effective hydration. The interaction between the water layer and the surface is crucial as well. The interaction energy E_{ghydr} between the water structure and the graphene sheet is directly proportional to the cumulative charge of these substructures (Figure 4B) with a slope of around 0.9 eV/e^- . This positive slope indicates repulsive interaction with increasing negative charge, which emphasizes that the interaction between water and graphene is mostly of electrostatic nature.

The importance of the hydration shell is neatly demonstrated by the comparison of the highly charged [2-22] cell (Figure 5). Besides charge buffering (comp. Table 2), electrostatic shielding is achieved by the introduction of water. The net of hydrogen bonds and the saturation of the acid oxygen atoms via coordination aid the adsorption. This yields a recumbent adsorption modus when water is present, while the upright modus is most stable without water (comp. Figure 5A,B). The difference is dramatic, which is evidently represented in the resulting adsorption energies.

3.4. Grand Canonical Potential. The adsorption energies, as presented earlier, do hold some valid information about the interaction between an adsorbate and a surface. However, since the hydration shell, the relative orientation of the molecules, and the (pH dependent) charge are crucial for the overall cell configuration, a more inclusive way of comparing the cells must be chosen.

To effectively compare the structure dependent thermodynamic stability of cells with different stoichiometries, the most common approach is to utilize the grand canonical potential³⁶ Ω . It is described by the total free energy F of a given cell and the chemical potentials μ of its parts N . In the case of DFT calculations, the real total free energies F are out of reach but can be reasonably approximated by the total cell energies E_{DFT} as received by DFT calculations. We assume the entropy contribution TS to be very similar in all cells and thus neglectable. Also, the temperature during the calculations is 0 K, thus practically negating the entropy term, leaving

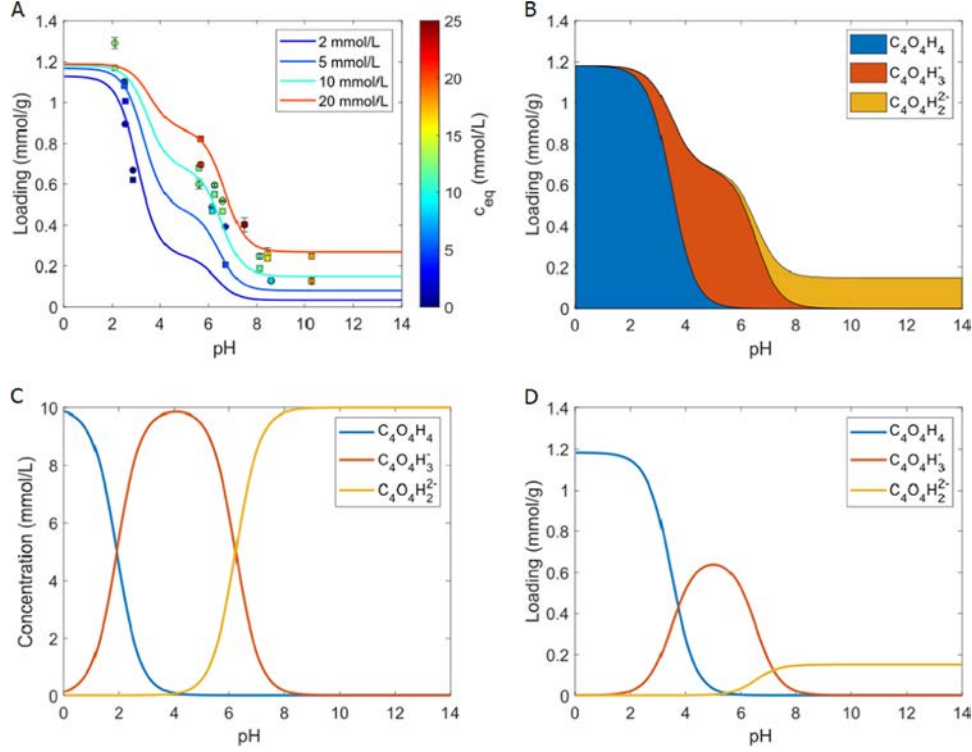


Figure 6. (A) pH dependence of the experimental and predicted loadings of maleic acid on activated carbon. Experimentally determined loadings are marked by circles and the markers for loadings calculated with the Langmuir model for the same conditions are squares. Furthermore, four isotherms for equilibrium concentrations of 2, 5, 10, and 20 mmol/L were calculated with the model and included. (B–D) Different aspects of the adsorbent and the solution for a constant total equilibrium concentration of maleic acid of 10 mmol/L in a pH range between 0 and 14. (B) The proportion of the three maleic acid species of the total loading. (C) The proportional concentrations of the three maleic acid species in solution for the same pH range and (D) the corresponding loadings of the maleic acid species on the carbon material as absolute values.

$$\Omega(\mu_i, N_i) \approx E_{\text{DFT}} - \sum_i \mu_i N_i \quad (7)$$

The chemical potentials of all components have to be assumed, either from experimental values or approximations via DFT calculations. To keep the comparability of the results, all chemical potentials used herein are calculated from DFT. For this, the same calculation environment and settings as for the actual cells were used (see Section 2.1). In the presented system of maleic acid on graphene, the chemical potentials of three elements, namely, carbon, oxygen, and hydrogen, must be considered. To obtain reasonable values for the chemical potential of carbon, we use the chemical potential of carbon from both a graphene sheet and CO_2 . Specifically, CO_2 is used as a reference point for the chemical potential of carbon in the carboxylic acid groups, while graphene is used as a reference for graphene and the reduced carbon backbone of maleic acid. For hydrogen and oxygen, the values are calculated from the respective molecular gases. We also consider the chemical potential of water as obtained for our quasi liquid phase (with $\Delta\mu_{\text{H}_2\text{O}} = 0.325$ eV as presented above).

$$\begin{aligned} \Omega(\mu_i, N_i)_{\text{DFT}} = & E_{\text{DFT}} - \mu(\text{C}_g)N(\text{C}_g) - \mu(\text{C}_{\text{acid}})N(\text{C}_{\text{acid}}) \\ & - \mu(\text{H}_2\text{O})N(\text{H}_2\text{O}) - \mu(\text{O})N(\text{O}) \\ & - \mu(\text{H}_{\text{CH}})N(\text{H}_{\text{CH}}) - \mu(\text{H}_{\text{acid}})N(\text{H}_{\text{acid}}) \end{aligned} \quad (8)$$

Importantly, for deriving the pH dependency of the relative stability of the cells, we only assume the COO-H hydrogen

atoms to be acidic protons. Their chemical potential is separated as follows

$$\mu(\text{H}_{\text{acid}}) = q_e \mu(e^-) + q_{\text{H}^+} \mu(\text{H}^+) \neq \text{const} \quad (9)$$

where the chemical potential of the electron is kept constant.³⁷ Additionally, following Himmel,³⁸ the chemical potential of the acidic protons is bound to the heat of solvation in the respective solvent and the pH via

$$\mu(\text{H}^+) = \Delta_{\text{solv}}G - [\text{pH} \cdot 0.05918 \text{ eV}] \quad (10)$$

In the presented case, all chemical potentials except for that of the proton are kept constant. This results in an overall grand canonical potential that only depends on the pH (Figure 2B).

In the range below pH 1.5 (Figure 2B), the grand canonical potential of the cell with two undissociated molecules of maleic acid [2–00] on the graphene sheet is most negative. In the intermediate range between pH 1.5 and 6.3, the cell with one 1 fold deprotonated molecule of maleic acid [1–01] is most favorable. In a more alkaline regime than pH 6.3, the configuration with two fully dissociated molecules of maleic acid [2–22] is the most stable. The pivot points found here are in very good agreement with the experimental $\text{p}K_a$ s of the organic molecule.³⁹

3.5. Experimental Results. To get a grasp of the affinity of maleic acid toward activated carbon powders, pH dependent adsorption capacities were determined in batch experiments for a pH range from 2 to 10 and initial concentrations between 10 and 30 mmol/L (Figure 6A). The experimentally determined pH dependent loadings are marked as filled circles

with the color showing the maleic acid concentration in solution.

Unfortunately, these experiments solely give information about the total amount of adsorbed maleic acid and the total concentration in solution, even though maleic acid has three dissociation stages. Therefore, we adapted the adsorption affinities of the presented multicomponent Langmuir model to our data with the resulting parameters shown in Table 1.

The affinity constant of the uncharged species is the highest, and with the increasing charge of the molecules, a decrease in the affinity constants was found. The main reason for this decrease is likely the charge itself,^{40,41} since each adsorbed molecule hampers further adsorption of charged maleic acid molecules on the carbon material due to the premise of electroneutrality. Consequently, the loading for 2 fold negatively charged maleic acid is smaller than the observed loading for 1 fold negatively charged maleic acid. The good accordance between the experiments and the model is reflected by a coefficient of determination of 0.93. For direct comparison, the calculated loadings are also plotted in Figure 6A in the form of colored squares. The corresponding pairs of circles and squares appear at the same pH and have the same color, which accounts for the total equilibrium concentration of maleic acid in solution. Furthermore, four isotherms were plotted for constant total concentrations of 2, 5, 10, and 20 mmol/L, also using the same color legend. Working with generally low concentrations is obviously mandatory for the applied model to be valid.

The isotherms show three plateaus, where the loading is almost constant. The formation of the plateaus is caused by the pH dependent relative abundance of each dissociation state in solution, as visualized in Figure 6C. In cases where mainly one species is available in solution, only this species can adsorb onto the carbon, resulting in a plateau of the loading in the respective pH ranges. Starting from pH 0, the end of the first plateau, indicating the first drop of the loading, occurs around pH 3. At first glance, this drop might be expected at a $pK_{a,1}$ of maleic acid of 1.92. Especially, since the drop after the second plateau occurs at a pH close to a $pK_{a,2}$ of 6.23. The difference is caused by the much higher ratio K_A/K_B in comparison to the ratio K_B/K_C , namely, 64 in comparison to 9. Therefore, the adsorption of uncharged maleic acid is still dominating up to pH 3, despite its concentration in solution being lower than that of the 1 fold deprotonated maleic acid. The high affinity of the carbon material toward uncharged maleic acid is also reflected by the fact that all adsorption plateaus of the isotherms at low pH (Figure 6A) are almost reaching a saturation loading q_{max} of 1.2 mmol/g. In contrast, the loading plateaus of the 1 fold negatively charged species in the interval $4 < \text{pH} < 6$ are ranging from approx. 0.3 to 0.9 mmol/g for different total equilibrium concentrations of maleic acid. The resulting pH dependent amount of adsorbed maleic acid on the carbon material is visualized in Figure 5B,D, which shows the loadings of all three maleic acid species for an equilibrium concentration of 10 mmol/L. Specifically, Figure 6B shows the second (turquoise) isotherm from Figure 6A with the surface under the curve colored according to the proportion of each maleic acid species adsorbed on the carbon material. The absolute amount of each species adsorbed to the carbon surface is shown in Figure 6D.

Competitive adsorption is a key factor, which makes the adsorption of the 1 fold charged species almost impossible as soon as the concentration of the uncharged maleic acid is high

enough (leading to a loading of around 1.2 mmol/g). In this case, most of the available binding sites (equal to q_{max}) are occupied and the adsorption of the 1 fold charged species is suppressed. This can be seen in Figure 6D, where for $\text{pH} = pK_{a,1} = 1.92$, only a negligible amount of 1 fold charged maleic acid is adsorbed. On the contrary, due to more available binding sites and thus less competition between the 1 fold and 2 fold charged species, a comparably high amount of the 2 fold charged species is adsorbed at $\text{pH} = pK_{a,2} = 6.23$.

4. DISCUSSION

4.1. Adsorption from the Aqueous Phase. To be able to compare the obtained values to the experimental findings, a frame of reference has to be set. Herein, a molecule of maleic acid with varying degrees of dissociation in a shell of 12 water molecules, surrounded by vacuum, was used. Again, the grand canonical potentials of these cells were calculated from the DFT energies and chemical potentials as presented above. When conducting the respective calculations of maleic acid in a water shell, it is important to note that the chemical potential of the electrons is no longer dependent on graphene. Instead, the chemical potential is approximated by gradually charging the water/maleic acid substructures. The BCA of the relaxed structures resulted in the partial charges of the substructures. The chemical potential of the electron was then calculated as the sum of the energies depending on the partial charges of the substructures.

For these calculations, the same cell (to ensure constant volume) and overall settings were used. Also, all other chemical potentials were kept constant. Thus, the heat of adsorption from the aqueous phase could be calculated from the pH dependent grand canonical potentials of the cells with and without graphene. The results are presented in the context of the experimental findings (Table 4).

Table 4. Gibbs Free Energy Changes Determined by DFT and by the Adaptation of the Langmuir Approach to Experiments in Comparison and the Results Normalized by the Lowest Gibbs Free Energy Change

maleic acid species	$\Delta\Omega_{\text{pH,DFT}}$ (kJ/mol)	$\Delta\Omega_{\text{pH,DFT}}$ scaled (kJ/mol)	ΔG° Langmuir (kJ/mol)
$\text{C}_4\text{O}_4\text{H}_4$	296.2	22.8	22.4
$\text{C}_4\text{O}_4\text{H}_3^-$	148.9	11.5	12.1
$\text{C}_4\text{O}_4\text{H}_2^{2-}$	118.6	9.1	6.6

To compare the determined Langmuir constants to the DFT results, the conversion of each value to affinities of the same unit is necessary. Therefore, the Gibbs free energy change (ΔG°) was calculated using the obtained Langmuir constants.⁴² Since the molecules in question are organic compounds, it is reasonable to neglect the activity of the molecules in solution resulting in the following equation

$$\Delta G^\circ = -RT \ln \left(K \cdot \left(1 \frac{\text{mol}}{\text{L}} \right) \right) \quad (11)$$

Furthermore, the results from DFT calculations were converted to comparable energy by multiplying the difference of the grand canonical potentials of the adsorbed and the solvated state at respective pH values (0, 4, and 12) with Avogadro's constant. The resulting Gibbs free energies are listed in Table 4.

The resulting changes in Gibbs free energy determined by the DFT calculation are obviously higher, but they show the same trend of decreasing stability with increasing molecular charge. Since the DFT calculations are not specifically conducted for the carbon material used for the batch experiments and the absolute energies depend on the used functionals, a direct comparison is valid after rescaling. Therefore, the values were linearly rescaled by an arbitrary factor of 13, leaving very similar results. This indicates high accordance between the theoretical part of this study and the experiments and pronounces the prediction strength of affinities by DFT.

With $4 \times 4 \times 1$ k points along the graphene sheet, the bond lengths, and angles unify as expected. The Bader charge analysis yielded a charge distribution that might appear unexpected at first glance: the graphene substructure always holds around 1 electron equivalent of charge. Due to the applied k points during the structural minimization, graphene is factually conductive along the plane. In analogy to a C_{60} buckyball, this plane can effectively buffer small charges.^{43,44} This ability is further displayed in the resulting energies of the substructure: when negative charges are applied, the total energy of graphene reduces by around 1 eV (higher stability). It is to note that with higher charges, the stabilization per charge equivalent decreases. The charge distribution itself arises from the fact that in the calculations, a systemic background charge is applied to the whole cell rather than bringing a respectively charged molecule into an uncharged system. The band gap along the plane normal of graphene therefore does not inhibit the charge transfer since there simply is no charge transfer process.

The independently set up cells with different amounts of maleic acid and respective dissociation states yield adsorption energies that suggest that maleic acid will (thermodynamically) “stick” the best in the medium pH range between 1.9 and 6.3. Still, the cells with lower surface coverage show the highest adsorption energies. This is presumably due to the fact that with higher coverage at the same degree of dissociation, the amount of charge per molecule of maleic acid increases because graphene will only buffer around 1 electron equivalent of charge. Stronger repulsive electrostatic interactions between the higher charged molecules and the partially charged surface lead to effectively less stable configurations. While the adsorption energies alone are the highest for the cells with 1 fold deprotonated maleic acid, the analysis of the grand canonical potential shows that the highest cell stability lies in the range of $\text{pH} < 1.5$. Despite the negligence of entropy in the calculations, this is in very good agreement with the experimental findings. In this low pH region, the experimental loadings are highest as well. The grand canonical potential, however, follows the experimental degree of dissociation more closely than the loading. The concentration dependency of the deprotonation, especially toward low initial concentrations of maleic acid (2 mmol/L, comp. Figure 6A, dark blue line), was not reproduced in the calculations. This is due to the cell sizes needed to model the corresponding dilutions being too big for reasonable calculation times. The second tipping point obtained in the grand canonical potentials (at pH 6.4) is also in good agreement with the experimental pKs. The overall trend of the grand canonical potentials, however, mimics the experimentally found total loadings, making the presented computational routine a viable method for modeling real systems. The difference between the adsorption energies and

the grand canonical potentials is related to the fact that in a system with three components (graphene—water—maleic acid), the interactions between all components contribute to the overall stability of the cell.

Notably, the two presented hydration energies E_{hydr} and E_{ghydr} show opposite charge dependencies: while the interaction between water and maleic acid becomes more favorable with increasing charge, the interaction between water and graphene becomes more repulsive. This is neatly explained by the nature of the solvent, the formation of hydrogen bonds, and the geometric changes of the organic molecule with increasing deprotonation.

A direct comparison of the experimental and theoretical parts of this study is possible for some key factors: the specific surface area of the experimentally used adsorbent was determined to be 909 m^2/g , while that of the graphene sheet used in the calculations was 1315 m^2/g (since only one side was loaded). The maximum loading of the carbonaceous material was 1.2 mmol/g in the experiment versus 1.74 mmol/g for cells with one and 3.47 mmol/g for cells with two molecules of maleic acid in the DFT calculations. Normalizing the loading to the specific surface yields a maximum loading of 1.32 $\mu\text{mol}/\text{m}^2$ in the experiments versus 1.33 and 2.65 $\mu\text{mol}/\text{m}^2$, respectively, in the calculations. The similarity suggests that the cells with only one molecule of maleic acid reflect the low pH range of the experiments quite accurately. To mirror the high pH range of the experiments with lower maximal loadings, significantly bigger cells would be needed. The computationally predicted coverages cannot be reached in the experiments, which is most likely due to the nature of the technically activated charcoal Carbopal. Unlike graphene surfaces, it contains a relatively high number of functional groups, mainly carboxyl groups. With the increase of the pH of the solution, these are being equally deprotonated, leading to a negatively charged surface. Simple electrostatic considerations explain why the adsorption is less favorable under these conditions. Furthermore, a partially functionalized surface provides different adsorption sites, where the adsorbate has different affinities. However, this difference does not prohibit the prediction of the overall trend in the adsorption behavior, when employing the herein presented method.

As shown in the energies and the structure (Figure 5), the hydration shell plays a crucial role in this system. While the uncharged states of the maleic acid could be effectively modeled without water, this model does not hold for highly dissociated maleic acid. Importantly, this must be considered when DFT is used, e.g., to parametrize molecular dynamics calculations, where charged molecules are allowed in equilibrium.

5. CONCLUSIONS

In the present study, the importance of solvent molecules for DFT models was shown. Especially, charged molecules, e.g., dissociated organic acids, exhibit contrary adsorption behaviors, depending on the solvent shell. The increasing computational capabilities of the current area allow for systematic corrections of model systems toward more realistic systems. At the same time, the thermodynamic properties of the systems can still be effectively modeled, as validated by the presented experiments.

AUTHOR INFORMATION

Corresponding Author

Peter Thissen – *Karlsruher Institut für Technologie (KIT), Institut für Funktionelle Grenzflächen (IFG), 76344 Eggenstein Leopoldshafen, Germany; orcid.org/0000 0001 7072 4109; Email: peter.thissen@kit.edu*

Authors

Nils Schewe – *Karlsruher Institut für Technologie (KIT), Institut für Funktionelle Grenzflächen (IFG), 76344 Eggenstein Leopoldshafen, Germany; orcid.org/0000 0001 6283 4834*

Robin Wagner – *Karlsruher Institut für Technologie (KIT), Institut für Funktionelle Grenzflächen (IFG), 76344 Eggenstein Leopoldshafen, Germany; orcid.org/0000 0002 7856 9390*

Matthias Franzreb – *Karlsruher Institut für Technologie (KIT), Institut für Funktionelle Grenzflächen (IFG), 76344 Eggenstein Leopoldshafen, Germany; orcid.org/0000 0003 3586 4215*

Notes

The authors declare no competing financial interest.

ACKNOWLEDGMENTS

Peter Thissen acknowledges the DFG for financial support.

REFERENCES

- (1) Brammen, M.; Fraga García, P.; Berensmeier, S. Carbon Nanotubes a Resin for Electrochemically Modulated Liquid Chromatography. *J. Sep. Sci.* **2017**, *40*, 1176–1183.
- (2) Knizia, M. W.; Vuorilehto, K.; Schrader, J.; Sell, D. Potential Controlled Chromatography of Short Chain Carboxylic Acids. *Electroanalysis* **2003**, *15*, 49–54.
- (3) Ponton, L. M.; Keller, D. W.; Siperko, L. M.; Hayes, M. A.; Porter, M. D. Investigation of Adsorption Thermodynamics at Electrified Liquid–Solid Interfaces by Electrochemically Modulated Liquid Chromatography. *J. Phys. Chem. C* **2019**, *123*, 28148–28157.
- (4) Trunzer, T.; Stummvoll, T.; Porzenheim, M.; Fraga García, P.; Berensmeier, S. A Carbon Nanotube Packed Bed Electrode for Small Molecule Electrosorption: An Electrochemical and Chromatographic Approach for Process Description. *Appl. Sci.* **2020**, *10*, No. 1133.
- (5) Yamini, Y.; Seidi, S.; Rezazadeh, M. Electrical Field Induced Extraction and Separation Techniques: Promising Trends in Analytical Chemistry – a Review. *Anal. Chim. Acta* **2014**, *814*, 1–22.
- (6) Karanfil, T.; Kilduff, J. E. Role of Granular Activated Carbon Surface Chemistry on the Adsorption of Organic Compounds. 1. Priority Pollutants. *Environ. Sci. Technol.* **1999**, *33*, 3217–3224.
- (7) Ortmann, F.; Schmidt, W. G.; Bechstedt, F. Attracted by Long Range Electron Correlation: Adenine on Graphite. *Phys. Rev. Lett.* **2005**, *95*, No. 186101.
- (8) Thierfelder, C.; Witte, M.; Blankenburg, S.; Rauls, E.; Schmidt, W. G. Methane Adsorption on Graphene from First Principles Including Dispersion Interaction. *Surf. Sci.* **2011**, *605*, 746–749.
- (9) Lazar, P.; Karlický, F.; Jurečka, P.; Kocman, M.; Otyepková, E.; Šafářová, K.; Otyepka, M. Adsorption of Small Organic Molecules on Graphene. *J. Am. Chem. Soc.* **2013**, *135*, 6372–6377.
- (10) Ghahghaey, Z.; Hekmati, M.; Darvish Ganji, M. Theoretical Investigation of Phenol Adsorption on Functionalized Graphene Using DFT Calculations for Effective Removal of Organic Contaminants from Wastewater. *J. Mol. Liq.* **2021**, *324*, No. 114777.
- (11) Ulstrup, S.; Schüller, M.; Bianchi, M.; Fromm, F.; Raidel, C.; Seyller, T.; Wehling, T.; Hofmann, P. Manifestation of Nonlocal Electron Electron Interaction in Graphene. *Phys. Rev. B* **2016**, *94*, No. 081403.
- (12) Laage, D.; Elsaesser, T.; Hynes, J. T. Water Dynamics in the Hydration Shells of Biomolecules. *Chem. Rev.* **2017**, *117*, 10694–10725.
- (13) Nothling, M. D.; Xiao, Z.; Bhaskaran, A.; Blyth, M. T.; Bennett, C. W.; Coote, M. L.; Connal, L. A. Synthetic Catalysts Inspired by Hydrolytic Enzymes. *ACS Catal.* **2019**, *9*, 168–187.
- (14) Ma, X.; Hortelão, A. C.; Patiño, T.; Sánchez, S. Enzyme Catalysis to Power Micro/Nanomachines. *ACS Nano* **2016**, *10*, 9111–9122.
- (15) Kim, T. H.; Kang, S. H.; Han, J. E.; Seo, E. J.; Jeon, E. Y.; Choi, G. E.; Park, J. B.; Oh, D. K. Multilayer Engineering of Enzyme Cascade Catalysis for One Pot Preparation of Nylon Monomers from Renewable Fatty Acids. *ACS Catal.* **2020**, *10*, 4871–4878.
- (16) J Thiele, M.; Davari, M. D.; Konig, M.; Hofmann, I.; Junker, N. O.; Mirzaei Garakani, T.; Vojcic, L.; Fitter, J.; Schwaneberg, U. Enzyme–Polyelectrolyte Complexes Boost the Catalytic Performance of Enzymes. *ACS Catal.* **2018**, *8*, 10876–10887.
- (17) Kresse, G.; Furthmüller, J. Efficient Iterative Schemes for Ab Initio Total Energy Calculations Using a Plane Wave Basis Set. *Phys. Rev. B* **1996**, *54*, 11169–11186.
- (18) Hacene, M.; Anciaux Sedrakian, A.; Rozanska, X.; Klahr, D.; Guignon, T.; Fleurat Lessard, P. Accelerating Vasp Electronic Structure Calculations Using Graphic Processing Units. *J. Comput. Chem.* **2012**, *33*, 2581–2589.
- (19) Hutchinson, M.; Widom, M. Vasp on a Gpu: Application to Exact Exchange Calculations of the Stability of Elemental Boron. *Comput. Phys. Commun.* **2012**, *183*, 1422–1426.
- (20) Kresse, G.; Joubert, D. From Ultrasoft Pseudopotentials to the Projector Augmented Wave Method. *Phys. Rev. B* **1999**, *59*, 1758–1775.
- (21) Monkhorst, H. J.; Pack, J. D. Special Points for Brillouin Zone Integrations. *Phys. Rev. B* **1976**, *13*, 5188–5192.
- (22) Perdew, J. P.; Burke, K.; Ernzerhof, M. Generalized Gradient Approximation Made Simple. *Phys. Rev. Lett.* **1996**, *77*, 3865–3868.
- (23) Grimme, S.; Antony, J.; Ehrlich, S.; Krieg, H. A Consistent and Accurate Ab Initio Parametrization of Density Functional Dispersion Correction (DFT-D) for the 94 Elements H–Pu. *J. Chem. Phys.* **2010**, *132*, No. 154104.
- (24) Grimme, S.; Ehrlich, S.; Goerigk, L. Effect of the Damping Function in Dispersion Corrected Density Functional Theory. *J. Comput. Chem.* **2011**, *32*, 1456–1465.
- (25) Castro Neto, A. H.; Guinea, F.; Peres, N. M. R.; Novoselov, K. S.; Geim, A. K. The Electronic Properties of Graphene. *Rev. Mod. Phys.* **2009**, *81*, 109–162.
- (26) Wagner, R.; Bag, S.; Trunzer, T.; Fraga García, P.; Wenzel, W.; Berensmeier, S.; Franzreb, M. Adsorption of Organic Molecules on Carbon Surfaces: Experimental Data and Molecular Dynamics Simulation Considering Multiple Protonation States. *J. Colloid Interface Sci.* **2021**, *589*, 424–437.
- (27) Swenson, H.; Stadie, N. P. Langmuir’s Theory of Adsorption: A Centennial Review. *Langmuir* **2019**, *35*, 5409–5426.
- (28) Whitley, D. A Genetic Algorithm Tutorial. *Stat. Comput.* **1994**, *4*, 65–85.
- (29) Weigand, C. Deskriptive Regressionsrechnung. In *Statistik Mit Und Ohne Zufall: Eine Anwendungsorientierte Einführung*; Springer Berlin Heidelberg: Berlin, Heidelberg, 2019; pp 131–155.
- (30) Backhaus, K.; Erichson, B.; Plinke, W.; Weiber, R. Regressionsanalyse. In *Multivariate Analysemethoden: Eine Anwendungsorientierte Einführung*; Springer: Berlin, Heidelberg, Germany, 2018; pp 57–124.
- (31) Sahu, S.; Rout, G. C. Band Gap Opening in Graphene: A Short Theoretical Study. *Int. Nano Lett* **2017**, *7*, 81–89.
- (32) Krukowski, S.; Kempisty, P.; Strąk, P. Fermi Level Influence on the Adsorption at Semiconductor Surfaces—Ab Initio Simulations. *J. Appl. Phys.* **2013**, *114*, No. 063507.

- (33) Tang, W.; Sanville, E.; Henkelman, G. A Grid Based Bader Analysis Algorithm without Lattice Bias. *J. Phys.: Condens. Matter* **2009**, *21*, No. 084204.
- (34) Thierfelder, C.; Hermann, A.; Schwerdtfeger, P.; Schmidt, W. G. Strongly Bonded Water Monomers on the Ice Ih Basal Plane: Density Functional Calculations. *Phys. Rev. B* **2006**, *74*, No. 045422.
- (35) Mohammadi Hafshejani, T.; Hohmann, S.; Nefedov, A.; Schwotzer, M.; Brenner Weiss, G.; Izadifar, M.; Thissen, P. Formation and Stability of Nontoxic Perovskite Precursor. *Langmuir* **2019**, *35*, 16217–16225.
- (36) Qian, G. X.; Martin, R. M.; Chadi, D. J. Stoichiometry and Surface Reconstruction: An Ab Initio Study of GaAs(100) Surfaces. *Phys. Rev. Lett.* **1988**, *60*, 1962–1965.
- (37) Zuluaga, S.; Manchanda, P.; Zhang, Y. Y.; Pantelides, S. T. Design of Optimally Stable Molecular Coatings for Fe Based Nanoparticles in Aqueous Environments. *ACS Omega* **2017**, *2*, 4480–4487.
- (38) Himmel, D.; Goll, S. K.; Leito, I.; Krossing, I. A Unified Ph Scale for All Phases. *Angew. Chem., Int. Ed.* **2010**, *49*, 6885–6888.
- (39) Lide, D. R. *CRC Handbook of Chemistry and Physics*; American Chemical Society: Boca Baton, 2004; Vol. 126, pp 1586.
- (40) Husson, S. M.; King, C. J. Multiple Acid Equilibria in Adsorption of Carboxylic Acids from Dilute Aqueous Solution. *Ind. Eng. Chem. Res.* **1999**, *38*, 502–511.
- (41) Zhang, K.; Zhang, L.; Yang, S. T. Fumaric Acid Recovery and Purification from Fermentation Broth by Activated Carbon Adsorption Followed with Desorption by Acetone. *Ind. Eng. Chem. Res.* **2014**, *53*, 12802–12808.
- (42) Liu, Y. Is the Free Energy Change of Adsorption Correctly Calculated? *J. Chem. Eng. Data* **2009**, *54*, 1981–1985.
- (43) Gust, D.; Moore, T. A.; Moore, A. L. Mimicking Photosynthetic Solar Energy Transduction. *Acc. Chem. Res.* **2001**, *34*, 40–48.
- (44) Guldi, D. M.; Fukuzumi, S. *Fullerenes: From Synthesis to Optoelectronic Properties*; Springer: Netherlands: Dordrecht, 2002.

Repository KITopen

Dies ist ein Postprint/begutachtetes Manuskript.

Empfohlene Zitierung:

Schewe, N.; Wagner, R.; Franzreb, M.; Thissen, P.
[Role of the Hydration Shell in the pH-Dependent Adsorption of Maleic Acid.](#)
2021. The journal of physical chemistry <Washington, DC> / C, 125.
doi: [10.5445/IR/1000135505](https://doi.org/10.5445/IR/1000135505)

Zitierung der Originalveröffentlichung:

Schewe, N.; Wagner, R.; Franzreb, M.; Thissen, P.
[Role of the Hydration Shell in the pH-Dependent Adsorption of Maleic Acid.](#)
2021. The journal of physical chemistry <Washington, DC> / C, 125 (22), 12305–12315.
doi: [10.1021/acs.jpcc.1c01765](https://doi.org/10.1021/acs.jpcc.1c01765)

Lizenzinformationen: [KITopen-Lizenz](#)